THE JOURNAL OF BIOLOGICAL CHEMISTRY VOL. 291, NO. 50, pp. 25764–25775, December 9, 2016


# The Orai1 Store-operated Calcium Channel Functions as a Hexamer*[S]◆

Received for publication, September 14, 2016, and in revised form, October 17, 2016 Published, JBC Papers in Press, October 25, 2016, DOI 10.1074/jbc.M116.758813

**Xiangyu Cai[‡1], Yandong Zhou[‡1,2], Robert M. Nwokonko[‡], Natalia A. Loktionova[‡], Xianming Wang[‡], Ping Xin[‡], Mohamed Trebak[‡], Youjun Wang[§], and Donald L. Gill[‡3]**

*From the [‡]Department of Cellular and Molecular Physiology, the Pennsylvania State University College of Medicine, Hershey, Pennsylvania 17033 and the [§]Beijing Key Laboratory of Gene Resources and Molecular Development, College of Life Sciences, Beijing Normal University, Beijing 100875, China*

**Edited by Roger Colbran**

**Orai channels mediate store-operated $Ca^{2+}$ signals crucial in regulating transcription in many cell types, and implicated in numerous immunological and inflammatory disorders. Despite their central importance, controversy surrounds the basic subunit structure of Orai channels, with several biochemical and biophysical studies suggesting a tetrameric structure yet crystallographic evidence indicating a hexamer. We systematically investigated the subunit configuration of the functional Orai1 channel, generating a series of tdTomato-tagged concatenated Orai1 channel constructs (dimers to hexamers) expressed in CRISPR-derived *ORAI1* knock-out HEK cells, stably expressing STIM1-YFP. Surface biotinylation demonstrated that the full-length concatemers were surface membrane-expressed. Unexpectedly, Orai1 dimers, trimers, tetramers, pentamers, and hexamers all mediated similar and substantial store-operated $Ca^{2+}$ entry. Moreover, each Orai1 concatemer mediated $Ca^{2+}$ currents with inward rectification and reversal potentials almost identical to those observed with expressed Orai1 monomer. In Orai1 tetramers, subunit-specific replacement with Orai1 E106A "pore-inactive" subunits revealed that functional channels utilize only the N-terminal dimer from the tetramer. In contrast, Orai1 E106A replacement in Orai1 hexamers established that all the subunits can contribute to channel formation, indicating a hexameric channel configuration. The critical $Ca^{2+}$ selectivity filter-forming Glu-106 residue may mediate Orai1 channel assembly around a central $Ca^{2+}$ ion within the pore. Thus, multiple E106A substitutions in the Orai1 hexamer may promote an alternative "trimer-of-dimers" channel configuration in which the C-terminal E106A subunits are excluded from the hexameric core. Our results argue strongly against a tetrameric configuration for Orai1 channels and indicate that the Orai1 channel functions as a hexamer.**

The members of the Orai family of ion channels are ubiquitously expressed among cell types and mediate "store-operated" $Ca^{2+}$ entry signals, crucial in the control of many responses including gene expression, cell growth, secretory events, and cell motility (1–3). Orai channels are highly $Ca^{2+}$-selective plasma membrane (PM)[4] channels activated through an elaborate intermembrane coupling mechanism by the $Ca^{2+}$-sensing STIM proteins of the endoplasmic reticulum (ER) (1–6). Alterations in the function of Orai channels and STIM proteins are implicated in a large number of immunological, muscular, and inflammatory disease states (1, 7–9). STIM1 undergoes a complex conformational rearrangement in the ER membrane in response to depletion of ER luminal $Ca^{2+}$, and then translocates into discrete ER-PM junctions where it attaches to the PM surface and is able to directly tether and activate PM Orai1 channels (1, 2, 4–6). The structural properties of Orai channels and STIM proteins and details of the molecular coupling they undergo are key to understanding their physiological activation, pharmacological modification, and pathophysiological role in disease states. Better understanding of the molecular coupling interface between STIM1 and Orai1 continues to emerge (10–12), and significant advances are being made in discerning the mechanism by which Orai1 channels are gated by STIM1 (13–15). Recent studies have also provided a better understanding of the arrangement, dynamics, and stoichiometry of STIM proteins and Orai channels during their activation and coupling (16–21).

Despite the many advances in identifying the molecular mechanisms of Orai channel function, considerable uncertainty still exists in some of the fundamental basic structural properties of Orai channels and how they become activated by STIM proteins. In particular, the multimeric assembly of the Orai1 channel, the most commonly expressed of the three-

* This work was supported in whole or part by National Institute of Health Grants R01 GM120783 and R01 GM109279. The authors declare that they have no conflicts of interest with the contents of this article. The content is solely the responsibility of the authors and does not necessarily represent the official views of the National Institutes of Health.

◆ This article was selected as a Paper of the Week.

[S] This article contains supplemental Figs. S1 and S2.

[1] Both authors contributed equally to this work.

[2] To whom correspondence may be addressed: Dept. of Cellular and Molecular Physiology, the Pennsylvania State University College of Medicine, 500 University Dr., Hershey, PA 17033. Tel.: 717-531-5892; Fax: 717-531-7667; E-mail: zhouyd@psu.edu.

[3] To whom correspondence may be addressed: Dept. of Cellular and Molecular Physiology, the Pennsylvania State University College of Medicine, 500 University Dr., Hershey, PA 17033. Tel.: 717-531-8567; Fax: 717-531-7667; E-mail: dongill@psu.edu.

[4] The abbreviations used are: PM, plasma membrane, ER, endoplasmic reticulum; STIM, stromal-interacting molecule; CRAC, $Ca^{2+}$ release-activating $Ca^{2+}$; gRNA, guide RNA; BAPTA, 1,2-bis(*o*-aminophenoxy)ethane-*N*,*N*,*N*′,*N*′-tetraacetic acid; Bis-Tris, 2-[bis(2-hydroxyethyl)amino]-2-(hydroxymethyl)propane-1,3-diol.

member mammalian Orai channel family, has remained a contentious issue (1, 2, 5, 6, 22, 23). Recent crystallographic evidence reveals that *Drosophila* Orai has a hexameric subunit structure, a result reinforced by cross-linking and chromatographic evidence (22). The four transmembrane domains of Orai channels are exceedingly conserved from *Drosophila* to human, and the pore-lining residues revealed from the crystal structure coincide closely with residues predicted to lie in the pore from elegant structure-function studies (24–27) that preceded the crystallization results. However, despite this congruity of structural understanding, several earlier studies revealed a fundamentally different, tetrameric subunit structure for Orai1. Thus, Shuttleworth and colleagues (28) compared the function of concatenated Orai1 channels (dimers, trimers, and tetramers) and concluded that the functional unit of the Orai1 channel is a tetramer. Shortly after, a number of other studies using a variety of approaches, including recovery after photobleaching, cross-linking, and electron microscopy, reported a similar tetrameric subunit structure for Orai channels (29–33). Reports have also suggested that Orai channels may exist as dimers, which could associate into tetramers (29, 33) or possibly hexamers (34). A seemingly more definitive study from Thompson and Shuttleworth (23) directly compared the functional channel properties of tetrameric and hexameric concatemers of Orai1. It was reported that only the Orai1 tetramer gave rise to the $Ca^{2+}$-selective, inwardly rectifying, $Ca^{2+}$ release-activated $Ca^{2+}$ current ($I_{CRAC}$), the hallmark of authentic Orai1 channel function. In contrast, the hexameric concatemer gave an essentially non-selective cation conductance that was distinct from $I_{CRAC}$, leading the authors to conclude that the hexameric Orai1 channel fails to replicate the function of endogenous CRAC channels (23).

Given the controversy in defining the functional Orai1 channel structure, we undertook a systematic investigation of the subunit configuration of the Orai1 channel. We generated a series of tdTomato-tagged concatenated Orai1 channel constructs containing from two to six Orai1 subunits. We expressed these concatemers in CRISPR-derived HEK cells in which endogenous Orai1 expression was eliminated. We confirmed that all of the Orai1 concatemers were PM-expressed and retained their concatemeric structure at the PM. Unexpectedly, the dimeric, trimeric, tetrameric, pentameric, and hexameric Orai1 constructs all mediated substantial store-operated $Ca^{2+}$ entry. Still more surprisingly, each one of the different concatemers mediated current with inward rectification and reversal potentials virtually identical to those observed with expressed Orai1 monomers. Replacement of specific subunits within each of the concatemers with Orai1 E106A "pore-dead" subunits revealed that the functional channels are predominantly formed from insertion of just the N-terminal pair of Orai1 subunits into the channel structure. The hexameric concatemer appears distinct from shorter concatemers in being able to at least partially form functional channels by itself. Our results argue strongly against a tetrameric configuration for Orai1 channels and provide evidence consistent with the conclusion that the functional Orai1 channel is hexameric.

## Results and Discussion

*Design and Expression of Orai1 Concatemers in a Null Background*—The recent controversy in understanding the molecular composition of Orai1 channels (22, 23) led us to examine the function of concatenated multimers of Orai1. To ensure that there was no interference from endogenous Orai1 channels, we expressed the Orai1 concatemers in HEK cells in which the expression of endogenous Orai1 channels was eliminated through CRISPR/Cas9 gene editing. As shown in supplemental Fig. S1*A*, endogenous Orai1 was entirely absent in these cells. The Orai1-deleted HEK cells (HEK-$O1^{ko}$) were transfected to stably express STIM1-YFP (HEK-$O1^{ko}S1^{+}$ cells) (supplemental Fig. S1, *B* and *C*). Using fura-2-loaded HEK-$O1^{ko}S1^{+}$ cells, the depletion of $Ca^{2+}$ stores with 2.5 $\mu$M ionomycin resulted in no detectable $Ca^{2+}$ entry in $Ca^{2+}$ add-back experiments (supplemental Fig. S1*D*). The lack of any store-operated $Ca^{2+}$ signals in these STIM1-overexpressing store-depleted cells reveals that there is no detectable $Ca^{2+}$ entry mediated by Orai1, Orai2, or Orai3 in the cells.

We made a series of Orai1 concatemers comprising two, three, four, five, or six subunits of Orai1 joined together with intervening 36-amino acid linker sequences (supplemental Fig. S2*A*). Each concatemer was tagged with the high fluorescence intensity tdTomato protein at the C terminus. Using the HEK-$O1^{ko}S1^{+}$ cells, we compared the plasma membrane expression and function of each of these Orai1 concatemers as well as tdTomato-tagged Orai1 monomer. Deconvolved *z* axis images revealed that each tagged Orai1 construct was expressed at the PM (Fig. 1*A*). We verified this by imaging cells 10 min after plating and prior to cells spreading, which provides enhanced PM visibility (supplemental Fig. S2*B*). It was important to assess whether the PM-expressed surface Orai1 concatemeric proteins were authentic in size or had undergone alteration or degradation. Cells expressing Orai1 monomer or each of the Orai1 concatemers were biotinylated, and then surface proteins were isolated with NeutrAvidin resin, and following elution, assessed by Western analysis with an Orai1 antibody as shown in Fig. 1*B*. Each construct was observed as a discrete protein with molecular mass corresponding closely to the calculated size of the tdTomato-linked concatemers (see the legend for Fig. 1*B*). We also examined the proportion of expressed Orai1 concatemeric protein in the non-biotinylated state, which appeared in the NeutrAvidin resin flow-through, corresponding to the non-PM-expressed concatemer. As shown in Fig. 1*C* for the Orai1 hexamer, considerably more protein (~70% of total) is expressed on the cell surface when compared with that within the cell.

*Orai1 Concatemers Function Identically Regardless of Subunit Length*—Having established the authentic cell surface expression of each Orai1 concatemer, we examined their function. Surprisingly, in each case (dimer, trimer, tetramer, pentamer, and hexamer), expression of the tagged Orai1 constructs resulted in large and comparable store-operated $Ca^{2+}$ entry, which matched almost exactly the rate and extent of $Ca^{2+}$ entry observed with the Orai1 monomer (Fig. 2, *A* and *B*). Non-transfected cells in each case showed no $Ca^{2+}$ entry. Considering previous results (23) in which only the Orai1 channel concate-

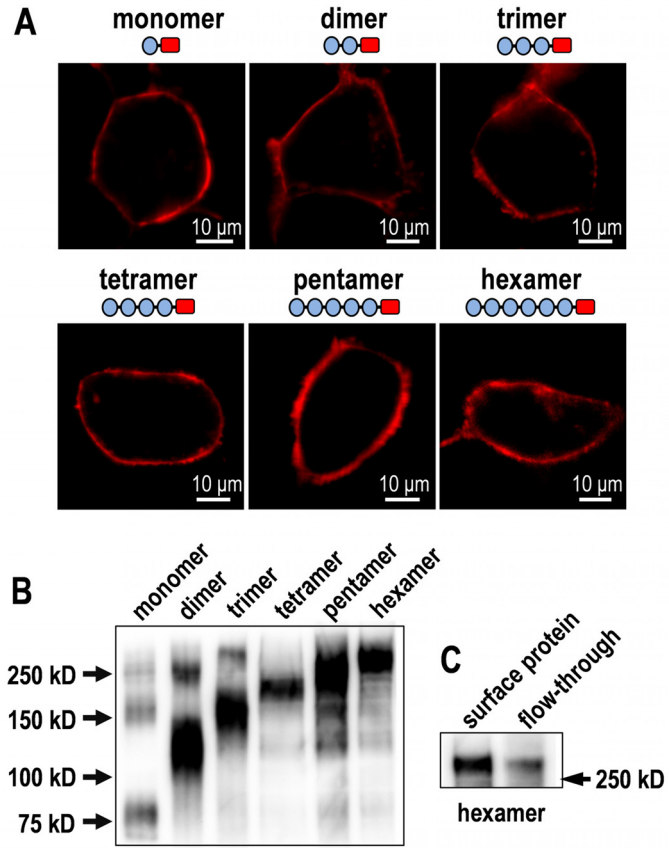


FIGURE 1. **Orai1 concatemers localize to the plasma membrane and exist in there with molecular masses corresponding to those predicted by their sequence.** *A*, deconvolved fluorescence images of HEK-O1$^{ko}$S1$^{+}$ cells expressing tdTomato-tagged Orai1 monomer, dimer, trimer, tetramer, pentamer, or hexamer constructs revealing their plasma membrane localization. *B*, Western blot of surface-isolated proteins isolated from the HEK-O1$^{ko}$S1$^{+}$ cells expressing tdTomato-tagged Orai1 monomers, dimers, trimers, tetramers, pentamers, or hexamers shown in *A*. Cells were biotinylated, and surface proteins were isolated with NeutrAvidin resin, eluted with DTT-containing sample buffer, and assessed by Western analysis with Orai1 antibody. The calculated molecular masses for tdTomato-linked Orai1 concatemers are: 91.2 kDa (monomer); 127.1 kDa (dimer); 163 kDa (trimer); 198.9 kDa (tetramer); 234.8 kDa (pentamer); 270.7 kDa (hexamer). *C*, comparison of the surface (PM) expression of Orai1 hexamer with that expressed elsewhere in the cell. Western blotting analysis used an Orai1 antibody to detect surface-biotinylated (*left*) and non-biotinylated (*right*) Orai1 protein derived from HEK-O1$^{ko}$S1$^{+}$ cells expressing tdTomato-tagged Orai1 hexamer. Following biotinylation of cells, lysates were applied to NeutrAvidin resin. The *flow-through lane* is the fraction that was not retained on NeutrAvidin resin. The *surface protein lane* is the fraction eluted with sample buffer/DTT after binding to NeutrAvidin resin. Details are given under "Experimental Procedures."

meric tetramer was reported to give rise to authentic CRAC channel function, we examined the current properties of each construct. As shown in Fig. 2*C*, the Orai1 monomer and each of the five concatemeric Orai1 constructs all gave rise to similar levels of authentic CRAC current with the same inwardly rectifying properties that define the operation of Orai1 channels (1). Indeed, from numerous recordings with each construct, the reversal potential for the inward current mediated by all five Orai1 concatemers lay within a narrow range (51–58 mV) (Fig. 2*D*) with no significant difference from that observed with monomeric Orai1 ($p < 0.05$).

In a previous study, dimeric and trimeric concatemers of Orai1 were observed to give rise to CRAC current, albeit smaller than the CRAC current observed with tetramer expression (28). It was concluded that the dimers and trimers could give rise to current through incorporation of monomers of endogenous Orai1 channel subunits to form tetramers. However, in the present case, we undertook all our experiments in the HEK-O1$^{ko}$S1$^{+}$ cells in which endogenous Orai1 was eliminated, and there was no functional detection of any other Orai channel activity. Thus, the currents observed are attributable to the expressed constructs *alone* and not any combinations with endogenous Orai1 channels. The more recent report from Thompson and Shuttleworth (23) indicated that a hexameric Orai1 concatemer gave a current-voltage relationship very different from authentic CRAC channels. In that report, the hexameric construct was observed to have less inward rectification and prominent outward currents at reversal potentials of +20 mV or above. In contrast, the tetrameric Orai1 construct in the same study gave rise to the strong inwardly rectifying current properties of an authentic CRAC current, very different from the properties of the hexamer. As shown in Fig. 2, *C* and *D*, we observe almost identical authentic CRAC current properties for both tetrameric and hexameric constructs, a result that is very different from the previous study (23). One possible difference could be the linker segments used: the earlier study used a 6-amino acid linker, whereas ours is 36 amino acids and is the same as that used to successfully attach STIM1 fragments to the Orai1 channel (16). It is possible that the longer linker could permit a more authentic configuration to be achieved in the multimers. However, in the earlier study (23), why there should have been a differential detrimental effect of a short linker *only* on the hexamer is difficult to reconcile. Also, in the previous studies and our own studies, the linkers are placed immediately upstream of the Orai1 N terminus of each conjoined Orai1 subunit. This N-terminal segment has ~70 amino acids that are redundant in the function of Orai1 channels (35, 36), and secondary structure analysis reveals little predicted secondary structure. These flexible 70 amino acids may therefore assist in linking the Orai1 units, making it still less clear why the 6-*versus* the 36-amino acid linker would selectively affect the function of Orai1 concatemers.

*E106A Pore-dead Subunit Substitution in Orai1 Dimers and Tetramers*—Next we sought to understand what could possibly allow all the concatemeric Orai1 constructs to function almost identically, and what we can determine about the nature of the functional Orai1 channel. The crystal structure of *Drosophila* Orai reveals it to be hexameric (22), and from its sequence similarity in critical transmembrane regions, the human Orai1 likely has a similar structure. We undertook functional studies on Orai1 concatemers in which we introduced one or more Orai1 residues that contained the E106A mutation. The Glu-106 residue is the crucial ion selectivity filter on the external surface of the channel pore (1), and its mutation to alanine completely prevents ion conductance (37). Initially, we substituted mutated Orai1 E106A subunits within the Orai1 dimer (Fig. 3*A*). Not surprisingly, mutation of either the first or the second subunit in the dimer to E106A (these constructs are termed "XO" or "OX," respectively) or mutation of both subunits in the dimer (XX) in each case almost completely prevented the function of the Orai1 dimer.

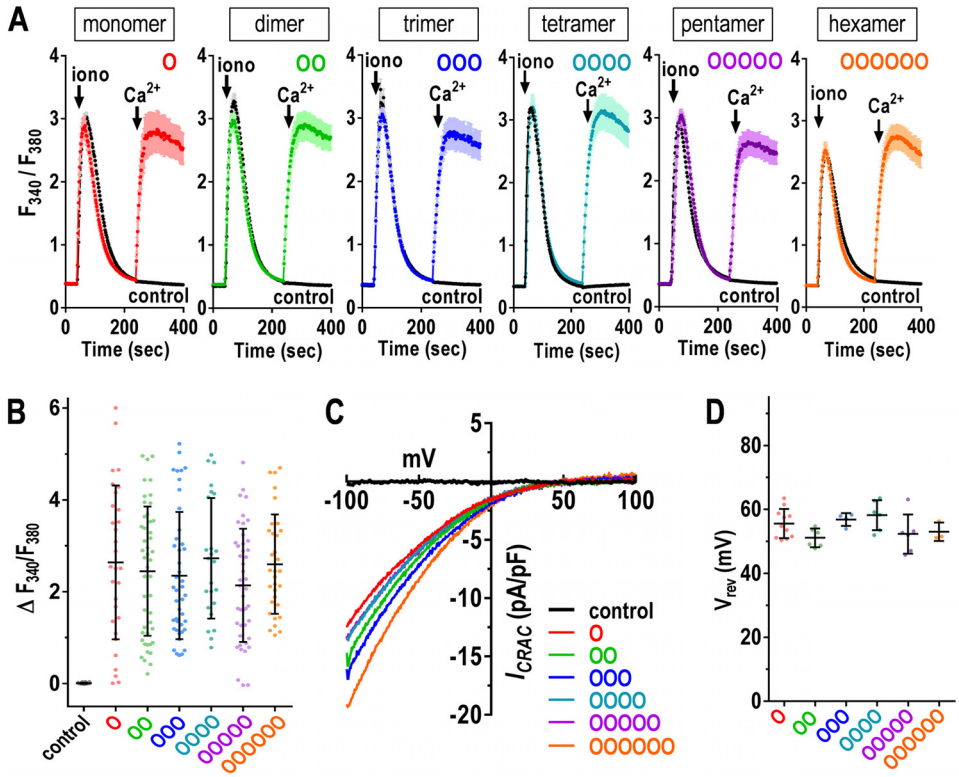


FIGURE 2. **Orai1 dimeric, trimeric, tetrameric, pentameric, and hexameric concatemers mediate store-operated $Ca^{2+}$ entry and CRAC current indistinguishable from that mediated by Orai1 monomer.** tdTomato-tagged Orai1 concatemer constructs were transiently expressed in HEK-O1$^{ko}$S1$^{+}$ cells. *A*, fura-2 ratiometric $Ca^{2+}$ add-back measurements for cells transfected with the concatemers shown. $Ca^{2+}$ stores were released upon the addition of 2.5 $\mu$M ionomycin in $Ca^{2+}$-free medium followed by the addition of 1 mM $Ca^{2+}$ (*arrows*). Traces (means ± S.E.) are representative of three independent experiments. *B*, summary scatter plots with means ± S.D. for peak $Ca^{2+}$ entry of all individual cells recorded in three independent experiments with the Orai1 concatemer constructs shown in *A*. *C*, representative I/V plots from whole-cell recordings from HEK-O1$^{ko}$S1$^{+}$ cells transiently expressing each of the tdTomato-tagged concatenated Orai1 constructs shown in *A*. *D*, summary statistics of the reversal potential measurements for each Orai1 concatemer construct described in *C*. Scatter plots are means ± S.D. for all the cells recorded in three independent experiments.

We also introduced E106A subunits into the Orai1 tetramer. Unexpectedly, the introduction of two E106A-mutated residues into the Orai1 tetramer caused entirely opposite results depending on the position of the mutated units. If the two N-terminal Orai1 residues were mutated to E106A (XXOO), the resulting construct was devoid of any $Ca^{2+}$ entry (Fig. 3*B*) or CRAC current (Fig. 3*C*). In contrast, if the two C-terminal Orai1 residues were mutated (OOXX), then the construct retained full $Ca^{2+}$ entry and normal CRAC current activity (Fig. 3, *B* and *C*). We considered whether the tdTomato tag at the C terminus would somehow influence the ability of these Orai1 constructs to assemble into functional channels. To test such possible directionality, we constructed similar Orai1 concatemeric tetramers that were N-terminally tagged with tdTomato. As shown in Fig. 3*D*, these constructs gave virtually identical results, the XXOO constructs having no function and the OOXX constructs mediating full $Ca^{2+}$ entry indistinguishable from the OOOO construct. An earlier report (38) had examined the effects of substituting Orai1 concatenated tetramers with subunits containing the pore-inactive R91W mutation found in patients with severe combined immunodeficiency disease. The results were shown only for an "XXOO" version of the substituted concatemer, and revealed that it had essentially negligible function in agreement with our results. However, in that study, the "OOXX" version of the concatemer was not examined.

*Substitution with E106A in the Orai1 Hexamer*—Because we know that E106A has a powerful and dominant inhibitory effect on Orai1 channel function, we interpreted these results to suggest that the two distal (C-terminal) residues of the tetramer might not be participating in formation of the functional channel. We also considered that, if the real functional Orai1 channel is a hexamer, the substitution of E106A units in the hexameric concatemer might have different functional consequences than in the tetrameric concatemer. We therefore compared the effects of substituting a single E106A unit in the first two positions of the concatemeric Orai1 hexamer as opposed to the Orai1 tetramer. As shown in Fig. 4*A*, a single E106A unit in the tetramer, regardless of whether in the first or second position (XOOO or OXOO), almost completely blocked store-operated $Ca^{2+}$ entry (SOCE). In contrast, substitution of E106A in either of the first two positions of the hexamer gave constructs with much more activity (Fig. 4, *B* and *C*). Substituted at the first position (XOOOOO), SOCE was observed to be ~15% of the wild-type hexameric channel. Substituted at the second position (OXOOOO), the channel was ~35% as functional as the wild-type hexamer (OOOOOO). This indicates that the hexamer is behaving quite differently from the tetramer. A comparison of the relative $Ca^{2+}$ entry for each of the first or second E106A-substituted dimers, tetramers, and hexamers is shown in Fig. 4*C*, from which it is clear that the hexamer is a special case.

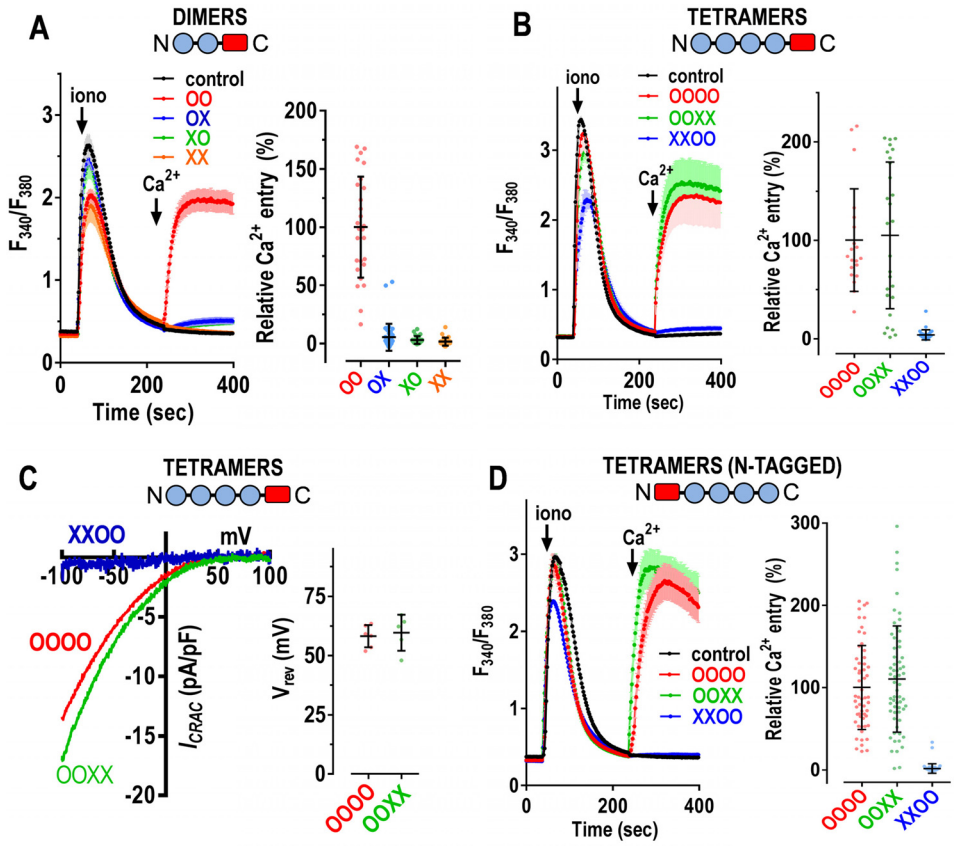


FIGURE 3. **Orai1 pore-inactive E106A subunit substitution in concatenated Orai dimers and tetramers.** *A*, fura-2 ratiometric $Ca^{2+}$ add-back measurements for HEK-O1$^{ko}$S1$^{+}$ cells expressing similar levels of the C-terminal tdTomato-tagged Orai1 dimer constructs shown. $Ca^{2+}$ stores were released upon the addition of 2.5 $\mu$M ionomycin in $Ca^{2+}$-free medium followed by the addition of 1 mM $Ca^{2+}$ (*arrows*). Traces are for wild-type Orai1 dimer (OO, *red*), dimer with Orai1 E106A substitution at the first (N-terminal) position (XO, *green*), second (C-terminal) position (OX, *blue*), E106A substitution at both positions (XX, *orange*), or untransfected control cells (*black*). *B*, fura-2 ratiometric $Ca^{2+}$ responses as in *A* with cells expressing similar levels of tdTomato-tagged Orai1 tetrameric concatemers, including the all-wild-type Orai1 tetramer (OOOO, *red*), Orai1 tetramer with the first subunit pair E106A-mutated (XXOO, *blue*), Orai1 tetramer with the second subunit pair E106A-mutated (OOXX, *green*), or untransfected control cells (*black*). *C*, representative I/V plots from whole-cell recordings from HEK-O1$^{ko}$S1$^{+}$ cells transiently expressing each of the tdTomato-tagged concatenated Orai1 tetramer constructs shown in *B*. Summary scatter plot (means ± S.D.) of reversal potential measurements taken from multiple I/V curves for the OOOO and OOXX constructs, as shown. Current for the XXOO construct was essentially zero. *D*, fura-2 ratiometric $Ca^{2+}$ responses as in *B* with cells expressing similar levels of tetrameric concatemers, but instead, all tagged with tdTomato at the N terminus. Traces are for the all-wild-type Orai1 tetramer (OOOO, *red*), Orai1 tetramer with the first subunit pair E106A-mutated (XXOO, *blue*), Orai1 tetramer with the second subunit pair E106A-mutated (OOXX, *green*), or untransfected control cells (*black*). For each of the results shown in *A*, *B*, and *D*, traces (means ± S.E.) are representative of three independent experiments. In each case, summary scatter plots with means ± S.D. of the percentage of peak $Ca^{2+}$ entry relative to wild type peak $Ca^{2+}$ entry are shown for all the cells derived from three independent experiments.

In further experiments, we examined a series of hexamers in which we substituted a single E106A unit at the third (OOXOOO), fourth (OOOXOO), fifth (OOOOXO), or sixth (OOOOOX) positions in the hexamer. The results shown in Fig. 5*A* reveal that each of these concatemers (especially with X at the fourth, fifth, and sixth positions) had substantial $Ca^{2+}$ entry. A summary of results for all the single X mutations in the Orai1 hexameric concatemer is shown in Fig. 5*A* (*right*). These results indicate that the position of the E106A unit does not make that much of a difference, with the exception of the first place (XOOOOO), which shows rather little function (Fig. 4, *B* and *C*). This is important information indicating that all the residues in the expressed Orai1 hexameric concatemer can contribute to its channel function. We continued investigation of the hexamer by substituting two adjacent E106A units at three different positions (Fig. 5*B*). When the E106A units were at the first and second position in the hexamer (XXOOOO), there was almost no function. However, when the E106A units were at the third and fourth positions (OOXXOO) or at the fifth and sixth positions (OOOOXX) in the hexamer, there was again substantial $Ca^{2+}$ entry function.

*Co-expression of Orai1 E106A Monomers with Orai1 Tetramers and Hexamers*—In an earlier report, the Orai1 tetramer was reported to be uniquely resistant to the dominant negative effects of co-expressing the pore-dead Orai1 monomer, E106Q (28). Thus, it was argued that the Orai1 tetramer was a structurally intact channel that could resist Orai1 monomer insertion, unlike other concatemers (for example, the Orai1 trimer) that were blocked as a result of Orai1 E106Q monomer incorporation. In contrast, we observed that the Orai1 E106A monomer co-expressed with the Orai1 tetrameric concatemer substantially blocked the function of the latter, and also had the same inhibitory effects on the Orai1 hexamer (Fig. 6, *A* and *B*). To be sure that this effect did not result from competition of the E106A monomer for STIM1 binding, we introduced the L273D mutation (which completely eliminates STIM1 binding (16, 39)) into the E106A monomer. This Orai1 E106A/L273D monomer still substantially blocked the func-

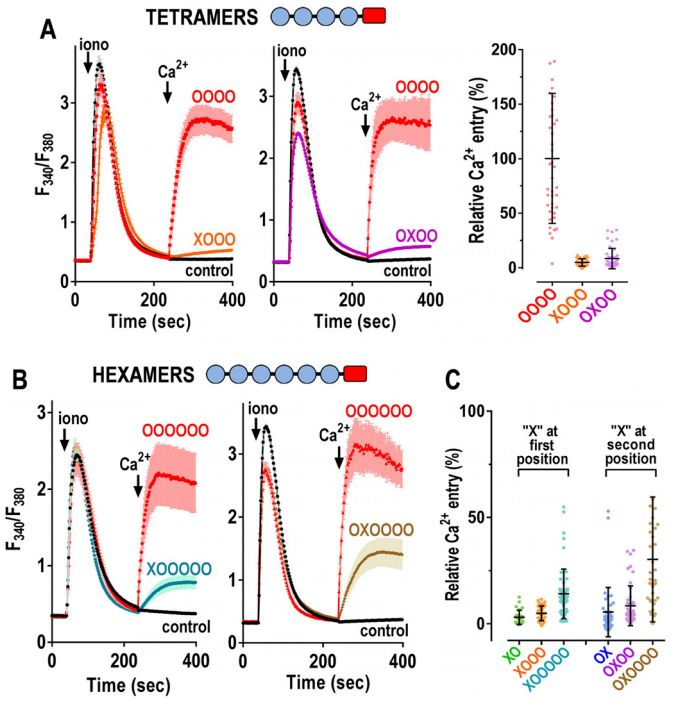


FIGURE 4. **The Orai1 tetrameric and hexameric concatemers differ in the effects of substituting Orai1 pore-inactive E106A subunits at the first or second positions.** *A*, fura-2 ratiometric $Ca^{2+}$ add-back measurements for HEK-O1$^{ko}$S1$^{+}$ cells expressing similar fluorescence levels of the C-terminal tdTomato-tagged Orai1 tetramers shown. $Ca^{2+}$ stores were released upon the addition of 2.5 $\mu$M ionomycin in $Ca^{2+}$-free medium followed by the addition of 1 mM $Ca^{2+}$ (*arrows*). *Left*, traces are for wild-type Orai1 tetramer (OOOO; *red*) or Orai1 tetramer substituted with E106A at the first position (XOOO, *orange*). *Middle*, traces are for wild-type Orai1 tetramer (OOOO, *red*) or Orai1 tetramer substituted with E106A at the second position (OXOO, *purple*). Untransfected control cells are shown for each experiment (*black*). Traces (means ± S.E.) are representative of three independent experiments. *Right*, summary scatter plots of peak $Ca^{2+}$ entry relative to wild type; results are means ± S.D. of all cells derived from three independent experiments. *B*, fura-2 ratiometric $Ca^{2+}$ add-back measurements for HEK-O1$^{ko}$S1$^{+}$ cells expressing similar levels of the C-terminal tdTomato-tagged Orai1 hexamers shown. $Ca^{2+}$ measurements were as in *A*. *Left*, traces are for wild-type Orai hexamer (OOOOOO, *red*) or Orai1 hexamer substituted with E106A at the first position (XOOOOO, *turquoise*). *Right*, traces are for wild-type Orai1 hexamer (OOOOOO, *red*) or Orai1 hexamer substituted with E106A at the second position (OXOOOO, *brown*). Untransfected control cells are shown for each experiment (*black*). Traces (means ± S.E.) are representative of three independent experiments. *C*, summary scatter plots of peak $Ca^{2+}$ entry relative to wild type; results are means ± S.D. of all cells from three independent experiments. The summary results for the XO and OX dimers from Fig. 3*A* are included for comparison.

tion of both the tetramer and the hexamer (Fig. 6, *C* and *D*). Thus, neither the tetramer nor the hexamer has any special exclusionary properties that lessen sensitivity to insertion and blockade by the monomer, a result further militating against the conclusion that the tetramer is the functional Orai1 channel configuration.

*A Model for the Functional Assembly of Orai1 Channel Concatemers*—The picture emerging from our concatemer studies shows a substantial difference between the operation of the dimer, tetramer, and hexamer. For dimers, both residues are essential and equal in their role in forming channels. For the tetramer, there is a complete distinction in the contribution of the first two (N-terminal) as opposed to the second two (C-terminal) subunits. In the hexamer, although all of the subunits can contribute to channel function, they do not contribute equally, and the double "XX" results reveal that the first two (N-terminal) subunits are more critical than the subsequent four residues. Based on the tetramer data, we conclude that channels are being formed by the concatemer in which some of the Orai1 subunits remain external from the functional channel core. Based on the strong crystallographic evidence that the channel is a hexamer (22), we postulate that the probable functional configurations of the dimers, tetramers, and hexamers are as shown in Fig. 7.

With the dimers, we assume that three dimers can assemble into a hexamer as a "trimer-of-dimers" (Fig. 7*A*). If both subunits in the dimer are E106A, there is no possibility of channel function. If one of the units in the dimer is E106A, there would be three E106A units in the hexamer, and this would likely also result in a channel with very little function. Indeed, the results with OX and XO (Fig. 3*A*) reveal very small $Ca^{2+}$ entry, but slightly more than observed with XX, which cannot form any functional channel protein. The lack of function of the XO and OX dimers indicates that functional channels are not formed from the assembly of six dimers each contributing just one functional monomer to the hexameric assembly. Thus, we conclude that the Orai channel may be assembled from dimers, in agreement with other studies (29, 33, 34) as well as with the crystallographic structure that reveals that Orai channels comprise a trimer-of-dimers (22).

With concatemeric tetramers, substitution with E106A at the first two N-terminal positions (XXOO) results in virtually no $Ca^{2+}$ entry (Fig. 3*B*). However, substituted at the third and fourth positions (OOXX), the channel has the same function as wild-type OOOO. Clearly, these two C-terminal residues of OOXX are not contributing to the hexamer and are likely extending out of the hexamer as depicted in Fig. 7*B*. Thus, we conclude that the N-terminal pair of residues in the tetramer is fed into a hexameric structure as a trimer-of-dimers, whereas the C-terminal pair remains external to the channel. Remarkably, the pair of subunits feeding into the hexamer is not altered by the position of the tdTomato tag. Thus, when we take this large fluorescent tag and place it on the N terminus instead of the C terminus of the Orai1 tetramer, the functional results with the tetramers are exactly the same (Fig. 3*D*). Hence, the dimers of Orai1 still feed into the hexamer from the N-terminal end, despite the presence of the bulky tdTomato residue immediately adjacent to the N terminus. This is not so unexpected because tdTomato-tagged Orai1 monomers themselves can form functional channels (Fig. 2) with tags present on each Orai1 unit in the hexameric channel.

If we did not have the hindsight of the hexameric channel crystal structure (22), would our results with the dimers and tetramers be consistent with the previously proposed Orai1 tetramer model (23, 28)? The dimer data would be explainable because if the dimers were simply combining to form tetrameric channels, the OX and XO constructs would have no function. However, our results with the tetramers reveal that they are clearly *not* forming simple tetrameric ring structures as concluded in the earlier studies (23, 28). Thus, there would be no explanation for the completely opposite effects of OOXX as opposed to XXOO (Fig. 3, *B–D*) under the tetramer theory. Also, the XOOO and OXOO tetramers might be expected to

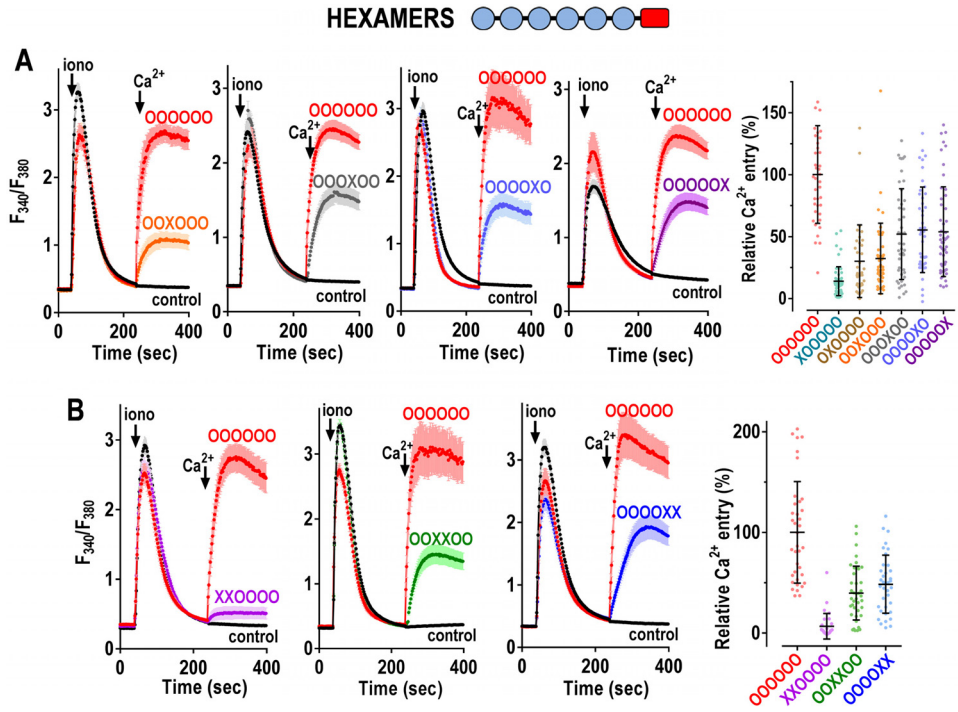


FIGURE 5. **Substitution of pore-inactive E106A subunits in the Orai1 hexamer reveals that all the subunits in the hexamer contribute to channel function.** *A*, fura-2 ratiometric $Ca^{2+}$ add-back measurements for HEK-O1$^{ko}$S1$^{+}$ cells expressing similar fluorescence levels of the C-terminal tdTomato-tagged Orai1 hexamers shown. $Ca^{2+}$ stores were released upon the addition of 2.5 $\mu$M ionomycin in $Ca^{2+}$-free medium followed by the addition of 1 mM $Ca^{2+}$ (*arrows*). In each case, traces for wild-type Orai1 hexamer (OOOOOO, *red*) are compared with traces for Orai1 hexamer substituted with E106A at the third (OOXOOO, *orange*), fourth (OOOXOO, gray), fifth (OOOOXO, *blue*), or sixth position (OOOOOX, *purple*). Untransfected control cells are also shown (*black*). *B*, $Ca^{2+}$ add-back measurements were as in *A* using hexamers substituted with pairs of E106A residues. In each case, traces for wild-type Orai1 hexamer (OOOOOO, *red*) are compared with traces for Orai1 hexamer substituted with two E106A subunits at the first and second (XXOOOO, *purple*), third and fourth (OOXXOO, *green*), or fifth and sixth position (OOOOXX, *blue*). Untransfected control cells are also shown (*black*). Traces (means ± S.E.) are representative of three independent experiments. Note that for the OOOOXO data (*A*, *third panel*), the wild-type trace (OOOOOO) is the same as that shown for the OXOOOO data (Fig. 4*B*, *right panel*) because the data were obtained in the same experiment. In each case, summary scatter plots of peak $Ca^{2+}$ entry relative to wild type are shown; results are means ± S.D. of all cells from three independent experiments.

have some function in a ring tetramer because only one out of the four subunits is deficient. However, these constructs are almost devoid of function (Fig. 4*A*).

Our results with the hexameric concatemers make a strong argument that the functional Orai1 channel is a hexamer, supporting the crystallographic identification of a hexameric channel structure. Thus, in the hexamers, substitution with a single E106A at any of the positions in the hexamer reduces function. However, the hexamer can still have good channel function, which would be expected with a single E106A substitution. Therefore, we conclude that the hexamer can indeed form a single ring that functions as a channel as shown in Fig. 7*C*. However, it seems that this is not the only functional assembly, and that the concatemeric hexamer can also form a functional trimer-of-dimers species equivalent to that formed by the tetramer, but now with four Orai1 units extending out from the hexameric core (Fig. 7*C*). This conclusion is strongly supported by the function of the double E106A-substituted hexamers shown in Fig. 5*B*. Thus, E106A subunits in the first two positions (XXOOOO) result in almost no channel function, whereas a pair of E106A units in the third and fourth, or fifth and sixth positions, results in significant channel function. This conclusion is reinforced by the observation that single E106A substitutions at different positions in the hexamer are not equal, those at the N terminus having more effect than those at the C terminus (Fig. 5*A*, *right*). If all the hexamer were in the ring configuration, there would be no positional difference observed with single E106A substitutions. If all the hexamer were in the trimer-of-dimers configuration, the two XOOOOO and OXOOOO constructs would have little activity. Thus, our hexameric concatemer is likely forming a combination of both configurations. Importantly, the hexamer is a special case and is able to tolerate a single X at the first (XOOOOO) or second position (OXOOOO) because at least some fraction of the hexamer can form as a hexameric ring. This sets it apart from the tetramer, which is unable to form a channel with a single X in either of the first two positions (XOOO, OXOO), because in contrast to the hexamer, the tetramer cannot form a complete ring assembly by itself.

The observation that Orai1 hexamers can function with one or more pore-inactive subunits has relevance to the expression of pore-inactive mutations (for example, R91W) in severe combined immune deficiency (SCID) patients. $Ca^{2+}$ entry responses in T cells derived from heterozygous disease carriers were relatively normal although diminished under conditions of lowered external $Ca^{2+}$ (40). Whether structures excluding pore-inactive subunits may result in the relatively normal behavior of Orai1 channels in the heterozygous case is an interesting possibility.

*The Selectivity Filter Glu-106 Appears Critical in Orai1 Channel Assembly*—Interestingly, increasing the number of E106A units beyond two provided some further perspective on

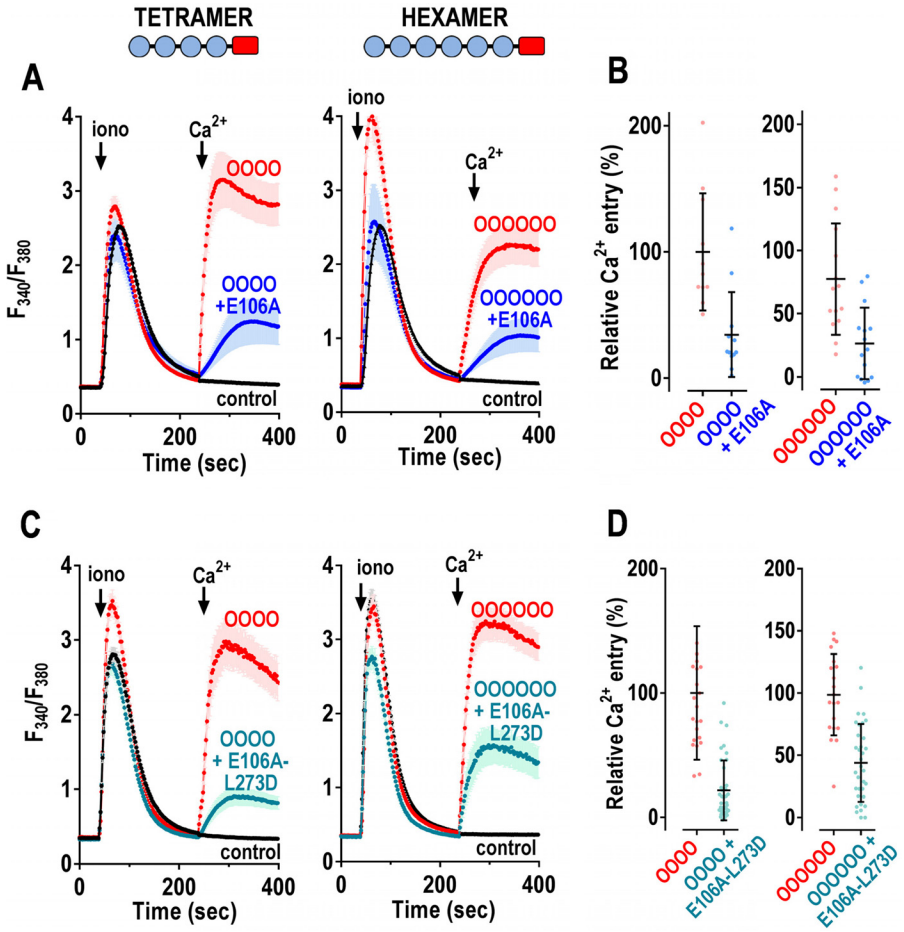


FIGURE 6. **The function of the Orai1 tetramer or Orai1 hexamer is substantially reduced by co-expression of pore-inactive Orai1 E106A monomer, and this effect is independent of any STIM1 binding of the monomer.** *A*, fura-2 ratiometric $Ca^{2+}$ add-back measurements for HEK-O1$^{ko}$S1$^{+}$ cells expressing similar levels of the C-terminal tdTomato-tagged Orai1 tetramer (*left*) or hexamer (*right*), either with (*blue traces*) or without (*red traces*) co-expression of Orai1 E106A monomer. $Ca^{2+}$ stores were released with 2.5 $\mu$M ionomycin in $Ca^{2+}$-free medium followed by the addition of 1 mM $Ca^{2+}$ (*arrows*). In each case, traces (means ± S.E.) are representative of all cells in two independent experiments. *B*, summary scatter plots of peak $Ca^{2+}$ entry in the presence of E106A monomer when compared with $Ca^{2+}$ entry without monomer; results are means ± S.D. of three independent experiments represented in *A*. *C*, exactly the same experimental design as in *A* except that the monomer used is the double mutant, Orai1 E106A/L273D, which is devoid of any ability to bind STIM1. Traces (means ± S.E.) are representative of three independent experiments. *D*, summary scatter plots of peak $Ca^{2+}$ entry in the presence of E106A monomer when compared with $Ca^{2+}$ entry without monomer; results are means ± S.D. of all cells in two independent experiments represented in *C*. Note that the levels of expression of tdTomato-tagged Orai1 tetramer or hexamer were not affected by Orai1 E106A monomer expression, and in each experiment, the level of tdTomato fluorescence, with or without monomer expression, was the same.

the function and assembly of the Orai1 channel. E106A units in the first three positions of the hexamer (XXXOOO) resulted in a nonfunctional channel (Fig. 8, *A* and *C*). Similarly, E106A substituted at the second, fourth, and sixth positions (OXOXOX) resulted in no function. These results would be expected, because regardless of the two alternative functional hexameric structures shown in Fig. 7*C*, these concatemer constructs would result in at least three E106A subunits in the channel and would therefore have little function. When we expressed the hexamer with three E106A subunits in the fourth, fifth, and sixth positions (OOOXXX), we obtained small but significant $Ca^{2+}$ entry (Fig. 8, *D* and *F*). This would again be expected because some functional channel likely arises through the trimer-of-dimers structure shown in Fig. 8*C*, whereas any ring structure would be nonfunctional by virtue of the three E106A units. Quite unexpectedly, introducing a fourth E106A residue into this hexamer (OOXXXX) resulted in high $Ca^{2+}$ entry, almost identical to that of the complete wild-type hexamer (OOOOOO) (Fig. 8, *E* and *F*). Thus, there is an extraordinary recovery of function by simply replacing the third subunit of the OOOXXX hexamer with E106A. This result appears counter-intuitive because the addition of a further non-functional channel subunit would be expected to further reduce rather than dramatically increase channel function.

This unexpected result has a most interesting possible rationale and may provide information about how the Orai1 channel assembles. We interpret the result to indicate that the OOXXXX construct has been forced to exist exclusively in the trimer-of-dimers configuration. Because the Glu-106 residue is itself the crucial $Ca^{2+}$ binding selectivity filter of the Orai1 channel pore, we postulate that by binding $Ca^{2+}$, this residue may also function to instigate the hexameric assembly of the Orai1 channel around a central $Ca^{2+}$ ion. We would assume that the OOOOOO hexamer would favor formation of the ring structure, although we do not know the proportion of ring *versus* trimer-of-dimers species present with that construct. As more E106A units are added to the C terminus, the channel not only becomes less conductive as a hexameric ring, but may also

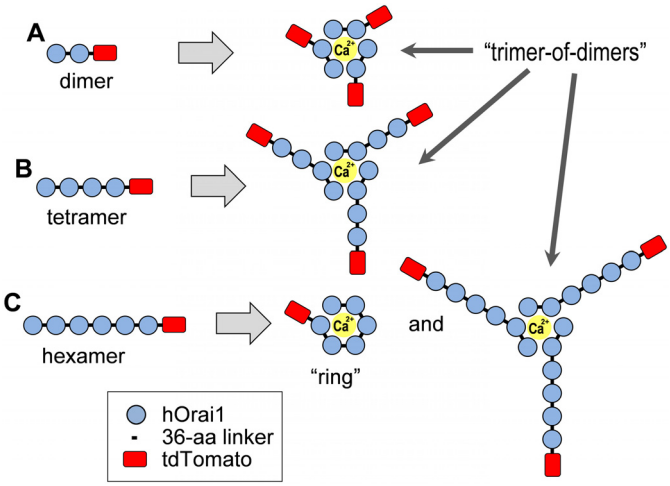


FIGURE 7. **Model of the possible assembly of concatenated Orai1 constructs to form functional hexameric channels.** The model depicts the ability of concatenated Orai1 dimers (*A*) or tetramers (*B*) to form functional hexameric channels through the insertion of three N-terminal dimers into a hexameric trimer-of-dimers complex. The concatenated Orai1 hexamer is distinct from the dimer and tetramer in being able to form a hexameric ring (*C*) in which all six of the subunits contribute to the function of the channel. The data suggest that the hexamer can additionally form a trimer-of-dimers complex similar to that formed by the tetramer. Details of the evidence and logic favoring formation of these functional assemblies are given under "Results and Discussion." *36-aa linker*, 36-amino acid linker.

become less susceptible to forming a ring nucleated by a $Ca^{2+}$ ion. By default, this would favor assembly of trimer-of-dimers species. With OOOOXX or OOOXXX, there may still be sufficient driving force for some ring formation, but such rings are with little or no channel function. Thus, three or four N-terminal O's might still be effective in preventing the trimer-of-dimer assembly as a result of promoting ring formation. However, with the OOXXXX structure, there is now no driving force for ring formation, and the assembly of trimer-of-dimers is strongly favored.

*Concluding Comments*—Our results provide strong support for the hexameric structure of the Orai1 channel. Moreover, our studies contradict previous studies that were interpreted to favor the tetramer model. First, concatemeric hexamers and tetramers both give rise to authentic CRAC currents, identical in properties to those mediated by the expression of Orai1 channels in native cells (Fig. 2). This directly refutes the previous evidence (23) that the tetramer is functionally distinct from the hexamer in mediating CRAC channel activity. Second, the function of dimers, trimers, and other multimers of Orai1 does not require the presence of endogenous Orai1 subunits to reconstitute functional CRAC channel activity as suggested earlier (28); thus, we observe the function of *all* Orai1 multimers in cells *devoid* of endogenous Orai1. Third, our experiments disprove the earlier report that the Orai1 tetramer is uniquely resistant to the dominant negative effects of co-expressing the pore-dead Orai1 monomer, E106Q (28).

Overall, our results provide functional data for the Orai1 channel that are highly consistent with the compelling structural data (22) from *Drosophila* Orai, indicating that the Orai1 channel is a hexamer. The crystal structure reveals that *Drosophila* Orai exists as a trimer-of-dimers, with each pair held together by hydrophobic interactions between the C termini of each of the two Orai subunits in the dimer. Such an assembly is consistent with other reports that indicate Orai channels are assembled from dimers (29, 33). Indeed, recent data indicate that PM dimers predominate in the resting state (90%) and can assemble into multimers up to hexamers, upon store depletion (34). This lends support to the evidence presented here that several combinations of concatemers may form hexamers through the assembly of dimers. When this happens, it seems that the dimers are always donated from the N terminus of concatemers. The presence of the E106A mutation may not only prevent the function of channels formed in this way, but it may also actively prevent the assembly of channels. This explains why the N-terminal Orai1 subunit in the concatemeric hexamer is the most susceptible to mutation (Figs. 4 and 5). We speculate that $Ca^{2+}$ binding to Glu-106 in this subunit may mediate a "seeding" role in Orai1 channel assembly; thereafter, the bound $Ca^{2+}$ functions as a template for channel assembly as described above. The strong inhibitory action we observe of E106A monomer co-expression with tetramers or hexamers (Fig. 6) may therefore reflect its dominant role in preventing channel assembly as well as channel function. Clearly, investigation of the subunit assembly of Orai1 channels will be an important area for future investigation.

## Experimental Procedures

*DNA Constructs*—The human Orai1 with 36-amino acid linker sequence was derived by PCR from the Orai1 S-S constructed previously (16). The DNA sequence was inserted into the pEGFP-N1 vector with the BamHI and XhoI restriction sites. The original EGFP tag was deleted using the BamHI and NotI restriction sites, and the tdTomato tag from ptdTomato-N1 with the same restriction sites was inserted into the construct to give ptdTomato-N1-Orai1. For the concatenated Orai1 dimer, the ptdTomato-N1-Orai1 was digested by BamHI and XhoI to obtain the Orai1-linker fragment, and this fragment was inserted into the same plasmid digested by BamHI and SalI. The trimer, tetramer, pentamer, and hexameric concatemers were constructed by repeating these digestion and ligation steps. Orai1 E106A mutations were derived using the QuikChange Lightning Site-Directed Mutagenesis Kit (Agilent; 210518).

*Generating Human ORAI1 Knock-out Cell Lines Using the CRISPR-Cas9 Nickase System*—Orai1 sequence-specific guide RNAs were inserted into the lentiCRISPR V2 vector (Addgene 52961) with the BsmBI restriction site to create a gRNA-Cas9-encoding plasmid. HEK cells were transfected with the gRNA-Cas9 plasmid using the cell line Nucleofector Kit (Lonza, VCA-1003) and the Amaxa Biosystems Nucleofector protocol (Lonza) according to the manufacturer's protocol. 48 h after transfection, cells were cultured in DMEM supplemented with 10% fetal bovine serum, penicillin, and streptomycin containing puromycin (2 $\mu$g/ml) (Gemini Bio Products, West Sacramento, CA) in 5% $CO_2$ at 37 °C. 6 days after puromycin selection, cells were collected and seeded at one cell per well into 96-well plates. Disruption of the *ORAI1* gene in individual colonies was detected using the Guide-it Mutation Detection Kit (Clontech Laboratories, 631443) and confirmed by sequencing, as well as Western blotting and functional responses

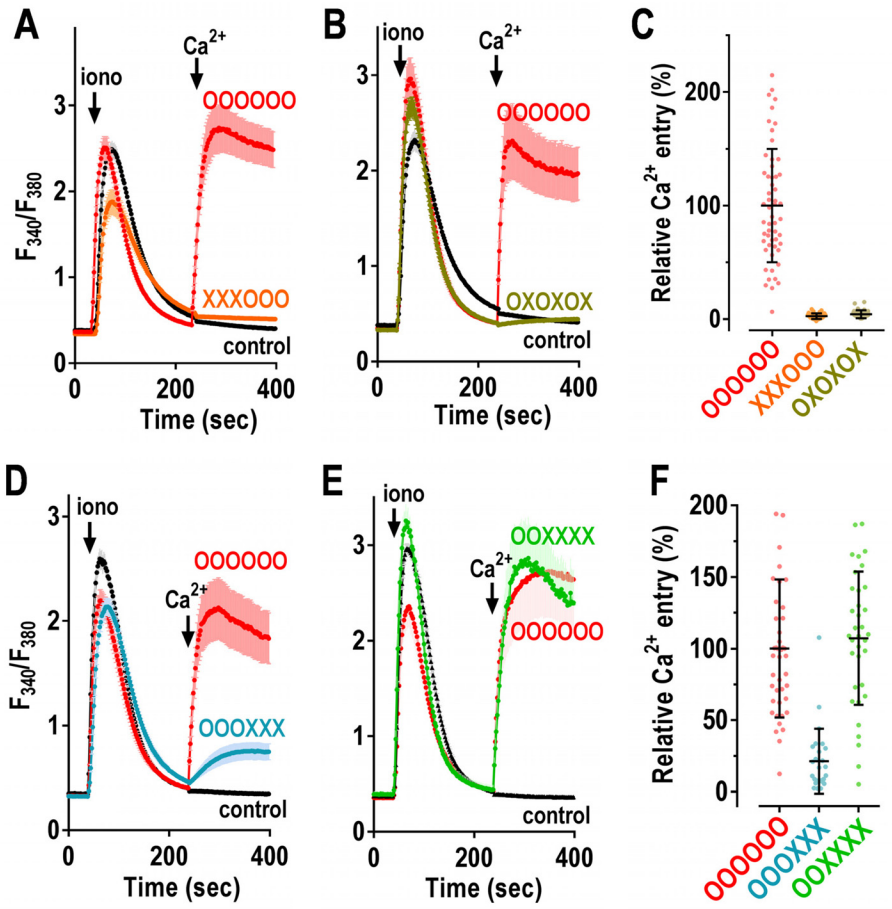


FIGURE 8. **The position and number of pore-inactive E106A subunits substituted in the Orai1 hexamer reveal profound differences in channel function likely reflecting different combinations of assembly as described under "Results and Discussion."** *A*, fura-2 ratiometric $Ca^{2+}$ add-back measurements for HEK-O1$^{ko}$S1$^{+}$ cells expressing similar levels of the C-terminal tdTomato-tagged Orai1 hexamers shown. $Ca^{2+}$ stores were released with 2.5 $\mu$M ionomycin in $Ca^{2+}$-free medium followed by the addition of 1 mM $Ca^{2+}$ (*arrows*). The trace for wild-type Orai1 hexamer (OOOOOO, *red*) is compared with that for Orai1 hexamer substituted with E106A at the first three positions (XXXOOO, *orange*). *B*, $Ca^{2+}$ add-back measurements as in *A* using Orai1 hexamer substituted with three E106A residues in the second, fourth, and sixth positions (OXOXOX, *olive*). Traces (means ± S.E.) are representative of three independent experiments. *C*, summary scatter plots of peak $Ca^{2+}$ entry when compared with wild type; results are means ± S.D. of all cells in three independent experiments represented in *A* or *B*. *D*, $Ca^{2+}$ add-back measurements as in *A* using Orai1 hexamer substituted with three E106A residues in the last three positions (OOOXXX, *cyan*). *E*, $Ca^{2+}$ add-back measurements as in *A* using Orai1 hexamer substituted with four E106A residues in the last four positions (OOXXXX; *green*). Traces (means ± S.E.) are representative of three independent experiments. *F*, summary scatter plots of peak $Ca^{2+}$ entry when compared with wild type; results are means ± S.D. of all cells in three independent experiments represented in *D* or *E*.

(supplemental Fig. S1). The *ORAI1* knock-out cell line generated was named HEK-O1$^{ko}$. The cell line STIM1-YFP-expressing HEK-O1$^{ko}$S1$^{+}$ was generated from the cells as described below. The oligonucleotides used for creating the Orai1 guide RNAs were: Orai1 gRNA 6F: 5′-CAC CGG TTG CTC ACC GCC TCG ATG T-3′; and Orai1 gRNA 6R: 5′-AAA CAC ATC GAG GCG GTG AGC AAC C-3′.

*Cell Culture and Transfection*—The stable HEK-O1$^{ko}$S1$^{+}$ cell line expressing STIM1-YFP was derived from HEK-O1$^{ko}$ cells using the transfection and selection methods described previously (41, 42). Cells were cultured in DMEM (Corning Cellgro) supplemented with 10% fetal bovine serum, penicillin, and streptomycin containing puromycin (2 $\mu$g/ml) (Gemini Bio Products) at 37 °C with 5% $CO_2$. All transfections were performed by electroporation at 180 V, 25 ms in 4-mm cuvettes (Molecular Bio-Products) using the Bio-Rad Gene Pulser Xcell system in OPTI-MEM medium as described previously (43). Experiments were all performed 18–24 h after transfection.

*Cytosolic $Ca^{2+}$ Measurements*—Cytosolic $Ca^{2+}$ levels were measured as described earlier (44) by ratiometric imaging using fura-2 (Molecular Probes). Cells were used 18–24 h after transfection, and then incubated with 2 $\mu$M fura-2 in buffer containing: 107 mM NaCl, 7.2 mM KCl, 1.2 mM $MgCl_2$, 1 mM $CaCl_2$, 11.5 mM glucose, 0.1% BSA, 20 mM HEPES, pH 7.2, for 30 min at room temperature, followed by treatment with fura-2-free solution for another 30 mins. Fluorescence ratio imaging was measured utilizing the Leica DMI6000B fluorescence microscope and Hamamatsu camera ORCA-Flash 4 controlled by SlideBook 6.0 software (Intelligent Imaging Innovations; Denver, CO) as described previously (45). Consecutive excitation at 340 nm ($F_{340}$) and 380 nm ($F_{380}$) was undertaken every 2 s, and emission fluorescence was collected at 505 nm. Intracellular $Ca^{2+}$ levels are shown as $F_{340}/F_{380}$ ratios obtained from groups of 8–25 single cells on coverslips. For the Orai1 concatemer experiments, data are shown for cells expressing a narrow range of tdTomato fluorescence to maximize the consistency of responses between cells. For each concatemer experiment, we simultaneously examined each set of mutants with the corresponding wild-type concatemer. The expression levels for wild-type and mutant concatemers were within a similar narrow

range of fluorescence intensity. All $Ca^{2+}$ imaging experiments were performed at room temperature, and representative traces of at least three independent repeats are shown. Scatter plots with means ± S.D. are shown for all the cells recorded.

*Deconvolved Fluorescence Image Analysis*—For the imaging of cells, we used the inverted Leica DMI6000B automated fluorescence microscope and Hamamatsu ORCA-Flash 4 camera controlled by SlideBook software to collect and analyze high resolution fluorescence images. For the PM localization studies of tdTomato-tagged Orai1 concatemers, stacks of 10–20 3D Z-axis image planes close to the cell-glass interface were collected at 0.35-$\mu$m steps. The no-neighbor deconvolution function of the SlideBook 6.0 software was used to analyze images and derive enhanced deconvolved images with minimized fluorescence contamination from out-of-focus planes. The tdTomato-tagged Orai1 concatemer images shown were typical of at least three independent analyses.

*Electrophysiological Measurements*—Whole-cell patch clamp recording was performed on HEK-$O1^{ko}S1^{+}$ cells transiently transfected with tdTomato Orai1 concatemer constructs, or not transfected, as described (11). To passively deplete ER $Ca^{2+}$ stores, the pipette solution contained: 135 mM cesium (aspirated), 10 mM HEPES, 8 mM $MgCl_2$, and 10 mM BAPTA (pH 7.2 with CsOH). The bath solution contained: 130 mM NaCl, 4.5 mM KCl, 5 mM HEPES, 10 mM dextrose, 10 mM tetraethylammonium chloride (TEA-Cl), and 20 mM $CaCl_2$ (pH 7.2 with NaOH). Currents were recorded in the standard whole-cell configuration using the EPC-10 amplifier (HEKA). Glass electrodes with a typical resistance of 2–4 megaohms were pulled using a P-97 pipette puller (Sutter Instruments). A 50-ms step to −100 mV from a holding potential of 0 mV, followed by a 50-ms ramp from −100 to 100 mV, was delivered every 2 s. Currents were filtered at 3.0 kHz and sampled at 20 kHz. A +10-mV junction potential compensation was applied to correct the liquid junction potential between the bath and pipette solutions. The current measure at −100 mV was used in I-V curves. All data were acquired with PatchMaster and analyzed using FitMaster and GraphPad Prism 6.

*Western Blotting and Biotinylation Analyses*—Cells were washed with ice-cold PBS and lysed on ice using lysis buffer (50 mM Tris-HCl, pH 8.0, 150 mM NaCl, 1% Nonidet P-40, and 1× protease inhibitor cocktail) for 30 min, followed by centrifugation at 14,000 × *g* for 10 min at 4 °C. Supernatants were collected, and protein was quantified using Bio-Rad DC kits. Proteins were resolved on 4–15% NuPAGE Bis-Tris precast gels and transferred to Bio-Rad Immuno-Blot PVDF membranes. After blocking in 5% nonfat milk for 1 h at room temperature, the membrane was incubated with primary antibody at 4 °C overnight. Membranes were washed three times in PBST (phosphate-buffered saline supplemented with 0.1% Tween-20) and incubated with secondary antibody for 1 h at room temperature. Subsequently, membranes were washed three times with PBST. Peroxidase activity was examined with Super-Signal West Pico Chemiluminescent Substrate (Thermo Scientific), and fluorescence was collected using the FluorChem M imager (ProteinSimple). Cell surface proteins were isolated after biotinylation using the Pierce Cell Surface Protein Isolation kit (Thermo Scientific, 89881). HEK-$O1^{ko}S1^{+}$ cells were transfected with ptdTomato-N1-Orai1 or each of the concatemers described (dimers through hexamers) for 24 h followed by washing cells twice with ice-cold PBS. Cells were incubated with 0.25 mg/ml Sulfo-NHS-SS-Biotin for 30 mins at 4 °C. Thereafter, quenching solution (Thermo Scientific, 1859386) was added to stop the reaction. Cells were collected and rinsed with TBS. Cells were then lysed in 200 $\mu$l of Lysis Buffer (Thermo Scientific, 1859387) on ice for 30 min and centrifuged at 10,000 × *g* for 10 mins at 4 °C. The supernatant containing biotinylated proteins was incubated with Immobilized Neutr-Avidin Gel (Thermo Scientific, 1859388) in the kit columns at room temperature for 1 h on a rocking platform. After centrifuging at 1,000 × *g* for 2 min, flow-through from the columns was collected and applied to gels to assess the level of non-biotinylated Orai1 concatemeric protein, that is, the levels of concatemer that did not reach the PM. Columns were washed three times with Wash Buffer (Thermo Scientific, 1859389), and the biotinylated protein was eluted with 200 $\mu$l of SDS-PAGE Sample Buffer with 50 mM DTT and resolved on 4–12% NuPAGE Bis-Tris precast gels (Life Technologies) as described above.

*Author Contributions*—Y. Z., X. C., and D. L. G. conceived the project, designed the experiments, undertook experiments, and wrote the manuscript. X. C., Y. Z., X. W., N. A. L., R. M. N., and P. X. performed the experiments and analyzed the data. Y. W. and M. T. provided valuable insight and helped write the manuscript. All authors reviewed the results and approved the final version of the manuscript.

## References


1. Prakriya, M., and Lewis, R. S. (2015) Store-operated calcium channels. *Physiol. Rev.* **95,** 1383–1436
2. Amcheslavsky, A., Wood, M. L., Yeromin, A. V., Parker, I., Freites, J. A., Tobias, D. J., and Cahalan, M. D. (2015) Molecular biophysics of Orai store-operated Ca channels. *Biophys. J.* **108,** 237–246
3. Shim, A. H., Tirado-Lee, L., and Prakriya, M. (2015) Structural and functional mechanisms of CRAC channel regulation. *J. Mol. Biol.* **427,** 77–93
4. Soboloff, J., Rothberg, B. S., Madesh, M., and Gill, D. L. (2012) STIM proteins: dynamic calcium signal transducers. *Nat. Rev. Mol. Cell Biol.* **13,** 549–565
5. Hogan, P. G. (2015) The STIM1-ORAI1 microdomain. *Cell Calcium* **58,** 357–367
6. Derler, I., Jardin, I., and Romanin, C. (2016) Molecular mechanisms of STIM/Orai communication. *Am. J. Physiol. Cell Physiol.* **310,** C643–C662
7. Kar, P., and Parekh, A. (2013) STIM proteins, Orai1, and gene expression. *Channels (Austin)* **7,** 374–378
8. Zhou, Y., Trebak, M., and Gill, D. L. (2015) Calcium signals tune the fidelity of transcriptional responses. *Mol. Cell* **58,** 197–199
9. Feske, S., Wulff, H., and Skolnik, E. Y. (2015) Ion channels in innate and adaptive immunity. *Annu. Rev. Immunol.* **33,** 291–353
10. Stathopulos, P. B., Schindl, R., Fahrner, M., Zheng, L., Gasmi-Seabrook, G. M., Muik, M., Romanin, C., and Ikura, M. (2013) STIM1/Orai1 coiled-coil interplay in the regulation of store-operated calcium entry. *Nat. Commun.* **4,** 2963
11. Wang, X., Wang, Y., Zhou, Y., Hendron, E., Mancarella, S., Andrake, M. D., Rothberg, B. S., Soboloff, J., and Gill, D. L. (2014) Distinct Orai-coupling domains in STIM1 and STIM2 define the Orai-activating site. *Nat. Commun.* **5,** 3183
12. Tirado-Lee, L., Yamashita, M., and Prakriya, M. (2015) Conformational changes in the Orai1 C-terminus evoked by STIM1 binding. *PLoS ONE* **10,** e0128622

13. Gudlur, A., Quintana, A., Zhou, Y., Hirve, N., Mahapatra, S., and Hogan, P. G. (2014) STIM1 triggers a gating rearrangement at the extracellular mouth of the ORAI1 channel. *Nat. Commun.* **5,** 5164
14. Palty, R., Stanley, C., and Isacoff, E. Y. (2015) Critical role for Orai1 C-terminal domain and TM4 in CRAC channel gating. *Cell Res.* **25,** 963–980
15. Zhou, Y., Cai, X., Loktionova, N. A., Wang, X., Nwokonko, R. M., Wang, X., Wang, Y., Rothberg, B. S., Trebak, M., and Gill, D. L. (2016) The STIM1 binding site nexus remotely controls Orai1 channel gating. *Nat. Commun.*, in press
16. Li, Z., Liu, L., Deng, Y., Ji, W., Du, W., Xu, P., Chen, L., and Xu, T. (2011) Graded activation of CRAC channel by binding of different numbers of STIM1 to Orai1 subunits. *Cell Res.* **21,** 305–315
17. Hoover, P. J., and Lewis, R. S. (2011) Stoichiometric requirements for trapping and gating of $Ca^{2+}$ release-activated $Ca^{2+}$ (CRAC) channels by stromal interaction molecule 1 (STIM1). *Proc. Natl. Acad. Sci. U.S.A.* **108,** 13299–13304
18. Rothberg, B. S., Wang, Y., and Gill, D. L. (2013) Orai channel pore properties and gating by STIM: implications from the Orai crystal structure. *Sci. Signal.* **6,** pe9
19. Wu, M. M., Covington, E. D., and Lewis, R. S. (2014) Single-molecule analysis of diffusion and trapping of STIM1 and Orai1 at endoplasmic reticulum-plasma membrane junctions. *Mol. Biol. Cell* **25,** 3672–3685
20. Perni, S., Dynes, J. L., Yeromin, A. V., Cahalan, M. D., and Franzini-Armstrong, C. (2015) Nanoscale patterning of STIM1 and Orai1 during store-operated $Ca^{2+}$ entry. *Proc. Natl. Acad. Sci. U.S.A.* **112,** E5533–E5542
21. Zhou, Y., Wang, X., Wang, X., Loktionova, N. A., Cai, X., Nwokonko, R. M., Vrana, E., Wang, Y., Rothberg, B. S., and Gill, D. L. (2015) STIM1 dimers undergo unimolecular coupling to activate Orai1 channels. *Nat. Commun.* **6,** 8395
22. Hou, X., Pedi, L., Diver, M. M., and Long, S. B. (2012) Crystal structure of the calcium release-activated calcium channel Orai. *Science* **338,** 1308–1313
23. Thompson, J. L., and Shuttleworth, T. J. (2013) How many Orai's does it take to make a CRAC channel? *Sci. Rep.* **3,** 1961
24. McNally, B. A., Yamashita, M., Engh, A., and Prakriya, M. (2009) Structural determinants of ion permeation in CRAC channels. *Proc. Natl. Acad. Sci. U.S.A.* **106,** 22516–22521
25. Zhou, Y., Ramachandran, S., Oh-Hora, M., Rao, A., and Hogan, P. G. (2010) Pore architecture of the ORAI1 store-operated calcium channel. *Proc. Natl. Acad. Sci. U.S.A.* **107,** 4896–4901
26. Zhang, S. L., Yeromin, A. V., Hu, J., Amcheslavsky, A., Zheng, H., and Cahalan, M. D. (2011) Mutations in Orai1 transmembrane segment 1 cause STIM1-independent activation of Orai1 channels at glycine 98 and channel closure at arginine 91. *Proc. Natl. Acad. Sci. U.S.A.* **108,** 17838–17843
27. McNally, B. A., Somasundaram, A., Yamashita, M., and Prakriya, M. (2012) Gated regulation of CRAC channel ion selectivity by STIM1. *Nature* **482,** 241–245
28. Mignen, O., Thompson, J. L., and Shuttleworth, T. J. (2008) Orai1 subunit stoichiometry of the mammalian CRAC channel pore. *J. Physiol.* **586,** 419–425
29. Penna, A., Demuro, A., Yeromin, A. V., Zhang, S. L., Safrina, O., Parker, I., and Cahalan, M. D. (2008) The CRAC channel consists of a tetramer formed by Stim-induced dimerization of Orai dimers. *Nature* **456,** 116–120
30. Ji, W., Xu, P., Li, Z., Lu, J., Liu, L., Zhan, Y., Chen, Y., Hille, B., Xu, T., and Chen, L. (2008) Functional stoichiometry of the unitary calcium-release-activated calcium channel. *Proc. Natl. Acad. Sci. U.S.A.* **105,** 13668–13673
31. Maruyama, Y., Ogura, T., Mio, K., Kato, K., Kaneko, T., Kiyonaka, S., Mori, Y., and Sato, C. (2009) Tetrameric Orai1 is a teardrop-shaped molecule with a long, tapered cytoplasmic domain. *J. Biol. Chem.* **284,** 13676–13685
32. Madl, J., Weghuber, J., Fritsch, R., Derler, I., Fahrner, M., Frischauf, I., Lackner, B., Romanin, C., and Schütz, G. J. (2010) Resting state Orai1 diffuses as homotetramer in the plasma membrane of live mammalian cells. *J. Biol. Chem.* **285,** 41135–41142
33. Demuro, A., Penna, A., Safrina, O., Yeromin, A. V., Amcheslavsky, A., Cahalan, M. D., and Parker, I. (2011) Subunit stoichiometry of human Orai1 and Orai3 channels in closed and open states. *Proc. Natl. Acad. Sci. U.S.A.* **108,** 17832–17837
34. Li, P., Miao, Y., Dani, A., and Vig, M. (2016) $\alpha$-SNAP regulates dynamic, on-site assembly and calcium selectivity of Orai1 channels. *Mol. Biol. Cell* **27,** 2542–2553
35. Derler, I., Plenk, P., Fahrner, M., Muik, M., Jardin, I., Schindl, R., Gruber, H. J., Groschner, K., and Romanin, C. (2013) The extended transmembrane Orai1 N-terminal (ETON) region combines binding interface and gate for Orai1 activation by STIM1. *J. Biol. Chem.* **288,** 29025–29034
36. McNally, B. A., Somasundaram, A., Jairaman, A., Yamashita, M., and Prakriya, M. (2013) The C- and N-terminal STIM1 binding sites on Orai1 are required for both trapping and gating CRAC channels. *J. Physiol.* **591,** 2833–2850
37. Prakriya, M., Feske, S., Gwack, Y., Srikanth, S., Rao, A., and Hogan, P. G. (2006) Orai1 is an essential pore subunit of the CRAC channel. *Nature* **443,** 230–233
38. Thompson, J. L., Mignen, O., and Shuttleworth, T. J. (2009) The Orai1 severe combined immune deficiency mutation and calcium release-activated $Ca^{2+}$ channel function in the heterozygous condition. *J. Biol. Chem.* **284,** 6620–6626
39. Muik, M., Frischauf, I., Derler, I., Fahrner, M., Bergsmann, J., Eder, P., Schindl, R., Hesch, C., Polzinger, B., Fritsch, R., Kahr, H., Madl, J., Gruber, H., Groschner, K., and Romanin, C. (2008) Dynamic coupling of the putative coiled-coil domain of ORAI1 with STIM1 mediates ORAI1 channel activation. *J. Biol. Chem.* **283,** 8014–8022
40. Feske, S., Gwack, Y., Prakriya, M., Srikanth, S., Puppel, S. H., Tanasa, B., Hogan, P. G., Lewis, R. S., Daly, M., and Rao, A. (2006) A mutation in Orai1 causes immune deficiency by abrogating CRAC channel function. *Nature* **441,** 179–185
41. Wang, Y., Deng, X., Zhou, Y., Hendron, E., Mancarella, S., Ritchie, M. F., Tang, X. D., Baba, Y., Kurosaki, T., Mori, Y., Soboloff, J., and Gill, D. L. (2009) STIM protein coupling in the activation of Orai channels. *Proc. Natl. Acad. Sci. U.S.A.* **106,** 7391–7396
42. Wang, Y., Deng, X., Mancarella, S., Hendron, E., Eguchi, S., Soboloff, J., Tang, X. D., and Gill, D. L. (2010) The calcium store-sensor, STIM1, reciprocally controls Orai and $Ca_V1.2$ channels. *Science* **330,** 105–109
43. Mancarella, S., Wang, Y., and Gill, D. L. (2011) Signal transduction: STIM1 senses both $Ca^{2+}$ and heat. *Nat. Chem. Biol.* **7,** 344–345
44. Soboloff, J., Spassova, M. A., Hewavitharana, T., He, L. P., Xu, W., Johnstone, L. S., Dziadek, M. A., and Gill, D. L. (2006) STIM2 is an inhibitor of STIM1-mediated store-operated $Ca^{2+}$ Entry. *Curr. Biol.* **16,** 1465–1470
45. Mancarella, S., Wang, Y., Deng, X., Landesberg, G., Scalia, R., Panettieri, R. A., Mallilankaraman, K., Tang, X. D., Madesh, M., and Gill, D. L. (2011) Hypoxia-induced acidosis uncouples the STIM-Orai calcium signaling complex. *J. Biol. Chem.* **286,** 44788–44798

**The Orai1 Store-operated Calcium Channel Functions as a Hexamer**

Xiangyu Cai, Yandong Zhou, Robert M. Nwokonko, Natalia A. Loktionova, Xianming Wang, Ping Xin, Mohamed Trebak, Youjun Wang and Donald L. Gill

*J. Biol. Chem. 2016, 291:25764-25775.*
*doi: 10.1074/jbc.M116.758813 originally published online October 25, 2016*

---